

## Effects of Precursor on Preparation and Properties of Nano-Crystalline Hopcalite Particles

N.M. DERAZ<sup>1,\*</sup> and OMAR H. ABD-ELKADER<sup>2,3</sup>

<sup>1</sup>Physical Chemistry Department, Laboratory of Surface Chemistry and Catalysis, National Research Center, Dokki, Cairo, Egypt

<sup>2</sup>Zoology Department, College of Science, King Saud University, Riyadh 11451, Kingdom of Saudi Arabia

<sup>3</sup>Electron Microscope and Thin Films Department, National Research Center, El- Behooth Street, 12622, Giza, Egypt

\*Corresponding author: E-mail: nmderaz@yahoo.com

Received: 15 October 2013;

Accepted: 20 November 2013;

Published online: 22 March 2014;

AJC-14977

X-ray diffraction techniques used to determine the structural properties of hopcalite nanoparticles. A mixture of hopcalite and its constituents can be prepared by ceramic method at 800 °C for 5 h. The spinel structure of hopcalite (Cu-Mn-O) confirms by infrared measurements. The copper precursors affect the formation and different properties of hopcalite. Solid state reaction between CuO resulted from copper nitrate with Mn<sub>2</sub>O<sub>3</sub> obtained from manganese carbonate brought about formation of spinel Cu<sub>1.5</sub>Mn<sub>1.5</sub>O<sub>4</sub> compound with subsequent formation of both Mn<sub>2</sub>O<sub>3</sub> and CuO. On the other hand, using of copper chloride as a source of CuO led to formation of both CuMn<sub>2</sub>O<sub>4</sub> and Mn<sub>2</sub>O<sub>3</sub>. The results showed that the change of precursor led to different changes in the structural properties of hopcalite solid including the crystallite size, lattice constant, unit cell volume, X-ray density, the distance between the reacting ions, ionic radii and bond lengths on tetrahedral and octahedral sites involved in the spinel structure.

**Keywords:** CuMn<sub>2</sub>O<sub>4</sub>, Cu<sub>1.5</sub>Mn<sub>1.5</sub>O<sub>4</sub>, Cu-Mn-O system, Hopcalite nanoparticles.

### INTRODUCTION

Hopcalite material, Cu<sub>x</sub>Mn<sub>3-x</sub>O<sub>4</sub>, is one of the most efficient materials, has wide commercial applications such as catalysts, electrodes, sensors and semiconductors<sup>1</sup>. The physical, catalytic and electrochemical properties of copper manganese spinel have been studied by several authors<sup>2-5</sup>. Cu-Mn-O system is very important to the respiratory protection in military, mining and space explorations due to its low cost and high activity. However, Cu-Mn oxides catalyst is efficient in many catalytic processes such as oxidation of both CO and alkanes, removal of volatile organic compounds, low-temperature NO reduction and other industrially important hydrogenation and oxidation reactions as well as the water-gas shift reaction<sup>6,7</sup>. This efficiency could be attributed to the redox couple<sup>8</sup> Cu<sup>2+</sup> + Mn<sup>3+</sup> = Cu<sup>+</sup> + Mn<sup>4+</sup>.

Electrochemical devices based on solid oxide fuel cells (SOFCs) convert the chemical energy to electrical energy depending upon high system efficiencies, environmental benefits and more adaptive fuel than either a conventional power plant or lower temperature polymer-based fuel cells<sup>9-11</sup>. Recently, spinel oxides based SOFCs' materials have received considerable attention because of their special physicochemical properties<sup>12-15</sup>. In fact, the common spinel oxides have thermal expansion coefficients closely matching to every part of

SOFCs<sup>16,17</sup>. Cu-Mn-O spinel has been proposed as a potential cathode<sup>18</sup>. The spinel oxides were used as the excellent potential candidate of the protective layer on ferric stainless steels to the cathode side<sup>19,20</sup>. Various authors reported that the protection layers of Co-Mn spinel oxides work well in the thermal and structural stability on the different type stainless steel interconnections<sup>21</sup>. Some investigators reported that Co-Mn-O and Cu-Mn-O systems were used as the protective layers between interconnections and cathode to improve the structural and thermal stability of the fuel cell stack<sup>15</sup>. The spinel oxides as the electrodes do not react with neighbor layers to yield high resistance phases, because the spinel oxides do not consist of rare-earth or alkaline-earth elements<sup>22</sup>. Therefore, the chemical capability is good between the spinel electrode and its neighbor layers. Opposite behavior was observed in case of the traditional perovskite oxides.

With the development of new soft chemistry routes, wide variety of single and mixed oxides can be prepared with a good control of the morphology and the grain size by changing transition metals or their respective content. This control is important for the application in coatings and particularly for optical properties. Controlling the surface chemical composition and mastering its modification at the nanometer scale are the critical issues for the high-added value applications involving nanoparticles. Various synthesis routes have been

employed for preparation of copper- manganese mixed oxides. These include co-precipitation, deposition-precipitation, impregnation, sol-gel and urea methods<sup>23, 24</sup>.

This study is devoted to the synthesis of copper manganite (hopcalite) by ceramic method. Another aim of this research is to obtain more information about effects of copper precursor on the formation and structural properties of hopcalite nanoparticles. Characterization of the final products can be achieved by XRD and IR techniques.

## EXPERIMENTAL

**Preparation of Cu/Mn mixed oxides:** Two samples of Cu/Mn mixed oxides were prepared by impregnating a known weight of finely powdered manganese carbonate with calculated amount of copper nitrate or copper chloride dissolved in the least amount of distilled water enough to make a paste. This paste was dried at 100 °C until constant weight and was then subjected to heat treatment in air for 5 h at 800 °C. The Cu/Mn mixed oxides prepared by copper nitrate and chloride are labeled as S1 and S2, respectively. The chemicals employed were of analytical grade and supplied by BDH Company. A general flowchart of the synthesis process is shown in Fig. 1.

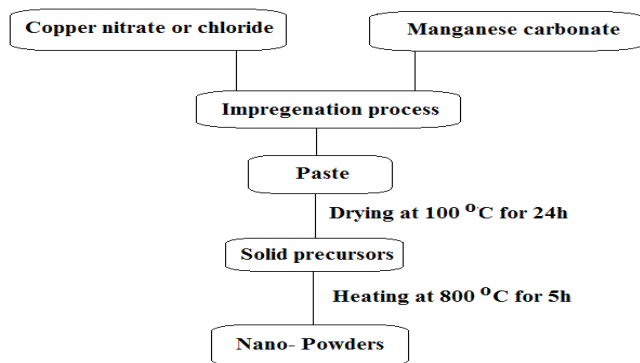


Fig. 1. Process flowchart for manufacturing the as prepared samples

**Characterization techniques:** An X-ray measurement of various mixed solids was carried out using a BRUKER D8 advance diffractometer (Germany). The patterns were run with  $\text{CuK}\alpha$  radiation at 40 kV and 40 mA with scanning speed in  $2\theta$  of  $2^\circ \text{ min}^{-1}$ .

The crystallite size of  $\text{CuMn}_2\text{O}_4$  or  $\text{Cu}_{1.5}\text{Mn}_{1.5}\text{O}_4$  present in the investigated solids was based on X-ray diffraction line broadening and calculated by using Scherrer equation<sup>25</sup>.

$$d = \frac{B\lambda}{\beta \cos\theta} \quad (1)$$

where  $d$  is the average crystallite size of the phase under investigation,  $B$  is the Scherrer constant (0.89),  $\lambda$  is the wave length of X-ray beam used,  $\beta$  is the full-width half maximum (FWHM) of diffraction and  $\theta$  is the Bragg's angle.

An infrared transmission spectrum of various solids was determined using Perkin-Elmer Spectrophotometer (type 1430). The IR spectra were determined from 1000 to 400  $\text{cm}^{-1}$ . Two mg of each solid sample were mixed with 200 mg of vacuum-dried IR-grade KBr. The mixture was dispersed by grinding for 3 min in a vibratory ball mill and placed in a steel die 13 mm in diameter and subjected to a pressure of 12 tonnes. The sample disks were placed in the holder of the double grating IR spectrometer.

## RESULTS AND DISCUSSION

**Crystallographic analysis:** The X- ray diffractograms for S1 and S2 samples are given in Fig. 2.

The results included in this figure can be summarized in some points as following: (i) The S1 sample showed all the diffraction peaks of CuO (JCPDS card No. 48-1548) and  $\text{Mn}_2\text{O}_3$  phases (JCPDS card No. 73-1826) and  $\text{Cu}_{1.5}\text{Mn}_{1.5}\text{O}_4$  (JCPDS card No. 70- 0262). This means that this sample consisted of  $\text{Mn}_2\text{O}_3$  (Bixbyite, major phase), CuO (Tenorite, minor phase) and  $\text{Cu}_{1.5}\text{Mn}_{1.5}\text{O}_4$  (Hopcalite, moderate phase). The crystallinity of these phases indicates the formation of well crystalline

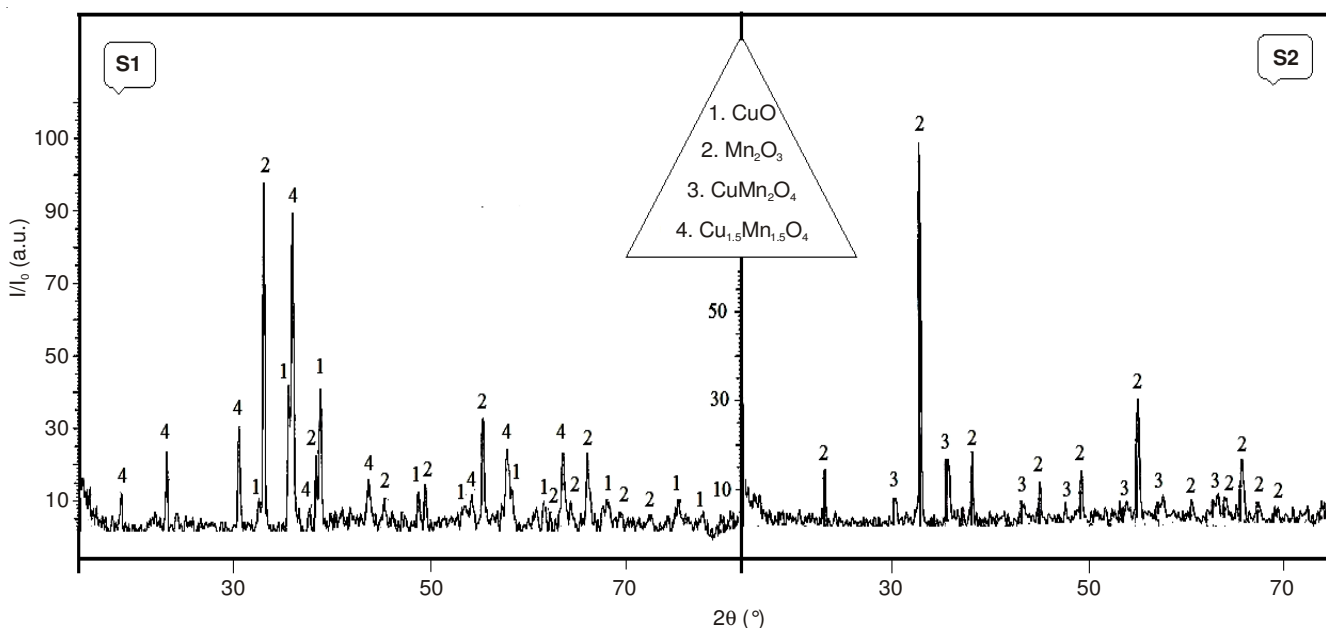


Fig. 2. XRD pattern for the S1 and S2 samples

mixed solids. (ii) The S2 sample consisted entirely of  $\text{CuMn}_2\text{O}_4$  (JCPDS card No. 84-0543) as a minor phase and  $\text{Mn}_2\text{O}_3$  as a major phase. The copper oxide is not present in XRD pattern of the S2 sample. This indicates the role of copper precursor in solid state reaction between Cu and Mn oxides. Hopcalite materials have spinel structure with two phases  $\text{Cu}_{1.5}\text{Mn}_{1.5}\text{O}_4$  and  $\text{CuMn}_2\text{O}_4$  depending upon preparation conditions. In fact,  $\text{Cu}_{1.5}\text{Mn}_{1.5}\text{O}_4$  and  $\text{CuMn}_2\text{O}_4$  phases have different planes (2 2 0), (3 1 1), (2 2 2), (4 0 0), (4 2 2), (3 3 3), (4 4 0) and (5 3 3) with the space group  $Fd\bar{3}m$ .

The calculated values of the crystallite size (d), lattice constant (a), unit cell volume (V) and X-ray density ( $D_x$ ) of both  $\text{Cu}_{1.5}\text{Mn}_{1.5}\text{O}_4$  and  $\text{CuMn}_2\text{O}_4$  phases, depending upon the data of X-ray, are given in Table-1.

TABLE-1  
CRYSTALLITE SIZE AND LATTICE PARAMETERS  
OF FOR HOPCALITE PHASES INVOLVED  
IN THE AS PREPARED SAMPLES

Samples	d (nm)	a (nm)	V (nm <sup>3</sup> )	$D_x$ (g/cm <sup>3</sup> )
S1	68	0.8286	0.5689	5.6425
S2	47	0.8307	0.5732	5.5015

It can be seen from Table-1 that the d and  $D_x$  values of  $\text{Cu}_{1.5}\text{Mn}_{1.5}\text{O}_4$  phase (68 nm) involved in the S1 sample is greater than that of  $\text{CuMn}_2\text{O}_4$  phase included in the S2 sample. However, the values of both V and a of  $\text{Cu}_{1.5}\text{Mn}_{1.5}\text{O}_4$  phase are smaller than that of  $\text{CuMn}_2\text{O}_4$  phase. On the other hand, the crystallite size of CuO phase involved in the S1 sample is 83 nm. The crystallite size of  $\text{Mn}_2\text{O}_3$  phase is 80 nm in the S1 sample and is 75 nm in the S2 sample. X-ray results were enabled us to calculate of the distance between the reacting ions ( $L_A$  and  $L_B$ ), ionic radii ( $r_A$ ,  $r_B$ ) and bond lengths (A-O and B-O) on tetrahedral (A) sites and octahedral (B) sites of  $\text{Cu}_{1.5}\text{Mn}_{1.5}\text{O}_4$  and  $\text{CuMn}_2\text{O}_4$  crystallites. The values of the previous parameters were summarized in Table-2.

**IR study:** Fig. 3 shows the IR transmission spectrum for the S2 samples in the range of 1000-400  $\text{cm}^{-1}$ . This figure showed displays three significant absorption bands. The vibration frequency located at 666  $\text{cm}^{-1}$  is characteristic of Mn-O stretching modes in tetrahedral sites; whereas the vibration frequency located at 583  $\text{cm}^{-1}$  corresponds to the distortion vibration of Mn-O in an octahedral environment. The third vibration band, located at 519  $\text{cm}^{-1}$ , can be attributed to the vibration of manganese species ( $\text{Mn}^{3+}\text{-O}$ ) in the octahedral site of hopcalite<sup>26-28</sup>. However, shoulder at 913  $\text{cm}^{-1}$  indicates the presence of Cu-O stretching modes in tetrahedral sites.

Normal cubic spinel Cu-Mn-O system can be prepared by ceramic method. In fact, the formation of Cu-Mn mixed oxides,  $\text{Cu}_x\text{Mn}_{3-x}\text{O}_4$ , requires prolonged heat with high temperature or post-heat treatment<sup>24,29</sup>. Copper manganite,  $\text{Cu}_x\text{Mn}_{3-x}\text{O}_4$ , compound can be crystallized in the form of  $\text{CuMn}_2\text{O}_4$  or  $\text{Cu}_{1.5}\text{Mn}_{1.5}\text{O}_4$  spinel phase depending upon the

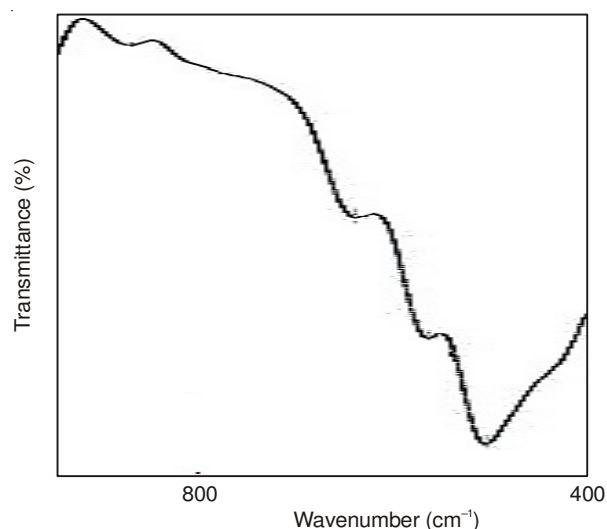


Fig. 3. IR spectrum of the S1 sample

thermal diffusion of Cu and Mn cations through the thin  $\text{Cu}_x\text{Mn}_{3-x}\text{O}_4$  film which covers the surfaces of grains of reacting oxides. In previous works, it was found that the thermal diffusion of the reacting cations and propagation of solid state reaction can be achieved by different factors such as doping, molar ratio, heat treatment, preparation conditions, metal precursors and also preparation methods<sup>30-32</sup>. Indeed, XRD measurements showed that the S2 sample, calcined at 800 °C, comprises  $\text{Mn}_2\text{O}_3$  (major phase) and  $\text{CuMn}_2\text{O}_4$  (minor phase). The proposed mechanism of formation of copper manganite,  $\text{CuMn}_2\text{O}_4$ , is according to the following stoichiometric reaction:



It was later reported that pure cubic spinel  $\text{CuMn}_2\text{O}_4$  could not be prepared at all<sup>33-35</sup>. Several authors reported that  $\text{Cu}^+$  can be formed during the sintering process of Cu-containing spinel materials. They proved that  $\text{Cu}^+$  ion prefers tetrahedral sites. However, any oxidation of  $\text{Cu}^+$  to  $\text{Cu}^{2+}$  on cooling in air does not cause an incorporation of the residual CuO into the spinel phase<sup>36</sup>. Opposite behavior was observed in case of the S2 sample synthesized from copper chloride depending upon the absence of any diffraction line refers to copper oxide. On the other hand, it was shown that the S1 sample quenched at 800 °C resulted in cubic spinel non-stoichiometric  $\text{Cu}_{1.5}\text{Mn}_{1.5}\text{O}_4$  phase with different amounts of  $\text{Mn}_2\text{O}_3$  and CuO as secondary phases<sup>37</sup>. The suggested mechanism of formation of copper manganite,  $\text{Cu}_{1.5}\text{Mn}_{1.5}\text{O}_4$ , is according to the following non-stoichiometric reaction:



This suggests that any oxidation of  $\text{Cu}^+$  to  $\text{Cu}^{2+}$  on cooling in air does not cause an incorporation of the residual CuO into the spinel phase<sup>9</sup>. Similar results carried out the neutron diffraction experiments on quenched  $\text{CuMn}_2\text{O}_4$  material reported to formation of  $\text{Cu}_{1.5}\text{Mn}_{1.5}\text{O}_4$  phase with partial inverse spinel

TABLE-2  
VALUES OF  $L_A$ ,  $L_B$ , A-O, B-O,  $r_A$  AND  $r_B$  FOR HOPCALITE PHASES INVOLVED IN THE AS PREPARED SAMPLES

Samples	$L_A$ (nm)	$L_B$ (nm)	A-O (nm)	B-O (nm)	$r_A$ (nm)	$r_B$ (nm)
S1	0.3588	0.2930	0.2009	0.1947	0.0659	0.0597
S2	0.3597	0.2937	0.2014	0.1952	0.0664	0.0602

structure<sup>34</sup>. These observations were established that using of copper nitrate in preparation of copper manganite led to formation of non-stoichiometric,  $\text{Cu}_{1.5}\text{Mn}_{1.5}\text{O}_4$ , form. This confirms the role of metal precursor in change of the crystallographic of product.

In XRD measurement, it is known that the peak position is indicative of the crystal structure. Also, peak intensities reflect the total scattering from each plane in the phase's crystal structure. However, the intensity, *i.e.* the peak area, is directly proportional to the amount and crystallite size of the phase studied. Both the S1 and S2 samples calcined at 800 °C are transformed to the spinel structured  $\text{Cu}_{1.5}\text{Mn}_{1.5}\text{O}_4$  and  $\text{CuMn}_2\text{O}_4$ , respectively, with some secondary phases. This process is assumed to be an isomorphous substitution of the  $\text{Mn}^{3+}$  and  $\text{Mn}^{4+}$  with  $\text{Cu}^+$  or  $\text{Cu}^{2+}$  depending upon the difference in the ionic radii of the reacting species<sup>38</sup>. Structural parameters for hopcalites involved in the S1 and S2 samples are summarized in Table-1. The standard characteristic peak (311) corresponding to  $\text{CuMn}_2\text{O}_4$  phase in the S2 sample is located at d-spacing 0.2505 nm. This peak shifted to the right, which displays the shortage of inter-planar spacing as shown in the S1 sample. Hence, this peak is located at d-spacing 0.2498 nm corresponding to  $\text{Cu}_{1.5}\text{Mn}_{1.5}\text{O}_4$  phase. The shorter inter-planar spacing confirm an isomorphous substitution for the copper and manganese cations during the calcination process, which leads to smaller crystallite size of  $\text{CuMn}_2\text{O}_4$  phase as shown in Table-1. This suggests that copper nitrate as precursor promotes grain growth in  $\text{Cu}_{1.5}\text{Mn}_{1.5}\text{O}_4$  more than the copper chloride precursor does. The crystallite size of  $\text{Mn}_2\text{O}_3$  in the S1 sample is higher than that in the S2 sample. This suggests that grains of Cu and  $\text{Mn}_2\text{O}_3$  are derived from less isomorphous substitution in the S1 sample. However, the final product of the S1 sample grows easier than that of the S2 sample by using copper nitrate precursor.

In spinel oxides, several authors reported that a variation in the distribution of cations in tetrahedral and octahedral sites resulted in significant changes in some of the physical properties of these oxides<sup>39-41</sup>. The spinel oxides have two or three main metal-oxygen bands in IR pattern. The highest band observed around 600  $\text{cm}^{-1}$ , correspond to intrinsic stretching vibrations of metal at the tetrahedral site, whereas the lowest band, usually observed around 400  $\text{cm}^{-1}$ , is assigned to octahedral-metal stretching. In this study, the vibration frequency located at 666  $\text{cm}^{-1}$  and 583  $\text{cm}^{-1}$  are characteristic of Mn-O stretching modes in tetrahedral and octahedral sites. The third vibration band, located at 519  $\text{cm}^{-1}$ , can be attributed to the vibration of manganese species ( $\text{Mn}^{3+}\text{-O}$ ) in the octahedral site of Cu-Mn-O spinel<sup>26-28</sup>. XPS measurements showed that copper can exist in both sites as monovalent and bivalent<sup>42</sup>. However, manganese can be bi-, tri- and tetra-valent. Indeed, the conservation of electro-neutrality in octahedral sites implies the formation of  $\text{Mn}^{4+}$  cations. Tetravalent manganese cations have a marked preference for octahedral sites. Navrotsky and Kleppa calculated, from thermodynamic measurements, the site preference energy of several cations within the spinel structure<sup>43</sup>. If  $\text{Cu}^{2+}$  and  $\text{Mn}^{3+}$  prefer octahedral environment,  $\text{Mn}^{2+}$  prefers tetrahedral one. Some authors have shown that  $\text{Cu}^{2+}$  can occupy both tetrahedral and octahedral sites<sup>42</sup>.

## Conclusion

Spinel copper manganites,  $\text{Cu}_{1.5}\text{Mn}_{1.5}\text{O}_4$  and  $\text{CuMn}_2\text{O}_4$ , were prepared by ceramic method *via* heating copper nitrate or copper chloride with manganese carbonate at 800 °C for 5 h. The results revealed that the manganite (hopcalite) synthesized from copper nitrate has the formula  $\text{Cu}_{1.5}\text{Mn}_{1.5}\text{O}_4$  while that prepared from copper chloride has the formula  $\text{CuMn}_2\text{O}_4$ . It was observed secondary phases with copper manganites. These phases are CuO and  $\text{Mn}_2\text{O}_3$  at using of copper nitrate precursors. Using of copper chloride led to formation of  $\text{Mn}_2\text{O}_3$  as a secondary phase with absence of CuO phase. These observations show the effect of copper precursor on the formation and properties of copper manganite. Various structural properties of the final products were investigated. Both the crystallite size and X-ray density of  $\text{Cu}_{1.5}\text{Mn}_{1.5}\text{O}_4$  phase are greater than that of  $\text{CuMn}_2\text{O}_4$  phase. Opposite behavior was observed in the case of lattice constant and unit cell volume for  $\text{Cu}_{1.5}\text{Mn}_{1.5}\text{O}_4$  and  $\text{CuMn}_2\text{O}_4$  phases. The distance between the reacting ions ( $L_A$  and  $L_B$ ), ionic radii ( $r_A$ ,  $r_B$ ) and bond lengths (A-O and B-O) on tetrahedral (A) sites and octahedral (B) sites of  $\text{Cu}_{1.5}\text{Mn}_{1.5}\text{O}_4$  and  $\text{CuMn}_2\text{O}_4$  crystallites were determined for both  $\text{Cu}_{1.5}\text{Mn}_{1.5}\text{O}_4$  and  $\text{CuMn}_2\text{O}_4$  phases. IR measurements confirm formation of spinel copper manganite.

## ACKNOWLEDGEMENTS

The authors extended their sincere appreciation to the Deanship of Scientific Research at King Saud University for its funding of this research through the Research Group Project no. RGP- VPP- 306.

## REFERENCES

1. H.A. Jones and H.S. Taylor, *J. Phys. Chem.*, **27**, 623 (1922).
2. I. Spassova, M. Khristova, D. Panayotov and D. Mehandjiev, *J. Catal.*, **185**, 43 (1999).
3. M. Trari, J. Topfer, P. Dordor, J.C. Grenier, M. Pouchard and J.P. Doumerc, *J. Solid State Chem.*, **178**, 2751 (2005).
4. C. Maunders, B.E. Martin, P. Wei, A. Petric and G.A. Botton, *Solid State Ionics*, **179**, 718 (2008).
5. B.E. Martin and A. Petric, *J. Phys. Chem. Solids*, **68**, 2262 (2007).
6. C. Yoon and D.L. Cocke, *Appl. Surf. Sci.*, **31**, 118 (1988).
7. F. Klauer, Paper presented at 1967 Mine Rescue Superintendents Conference (National Coal Board), Published by the Auergesellschaft GMBH, Berlin (1967).
8. A.A. Mirzaei, H.R. Shaterian and M. Kaykhaii, *Appl. Surf. Sci.*, **239**, 246 (2005).
9. N.Q. Minh, *J. Am. Ceram. Soc.*, **76**, 563 (1993).
10. B.C.H. Steele and A. Heinzl, *Nature*, **414**, 345 (2001).
11. E.D. Wachsman, C.A. Marlowe and K.T. Lee, *Energy Environ. Sci.*, **5**, 5498 (2012).
12. W.Z. Zhu and S.C. Deevi, *Mater. Sci. Eng. A*, **348**, 227 (2003).
13. A.J. Jacobson, *Chem. Mater.*, **22**, 660 (2010).
14. Z.G. Yang, G.G. Xia, G.D. Maupin and J.W. Stevenson, *Surf. Coat. Technol.*, **201**, 4476 (2006).
15. P. Wei, X.H. Deng, M.R. Bateni and A. Petric, *Corrosion*, **63**, 529 (2007).
16. Z.G. Yang, K.S. Weil, D.M. Paxton and J.W. Stevenson, *J. Electrochem. Soc.*, **150**, A1188 (2003).
17. N. Shaigan, W. Qu, D.G. Ivey and W.X. Chen, *J. Power Sources*, **195**, 1529 (2010).
18. Q. Zhang, B.E. Martin and A. Petric, *J. Mater. Chem.*, **18**, 4341 (2008).
19. X.S. Xin, S.R. Wang, J.Q. Qian, C.C. Lin, Z.L. Zhan and T.L. Wen, *Int. J. Hydrogen Energy*, **37**, 471 (2012).
20. S.R. Akanda, M.E. Walter, N.J. Kidner and M.M. Seabaugh, *J. Power Sources*, **210**, 254 (2012).

21. Z.G. Yang, G.G. Xia, X.H. Li and J.W. Stevenson, *Int. J. Hydrogen Energy*, **32**, 3648 (2007).
22. M.K. Mahapatra and K. Lu, *Int. J. Hydrogen Energy*, **35**, 11908 (2010).
23. A.A. Mirzaei, H.R. Shaterian, M. Habibi, G.J. Hutchings and S.H. Taylor, *Appl. Catal. A*, **253**, 499 (2003).
24. M. Jobbágy, F. Mariño, B. Schönbrod, G. Baronetti and M. Laborde, *Chem. Mater.*, **18**, 1945 (2006).
25. B.D. Cullity, *Elements of X-ray Diffraction*, Addison-Wesley Publishing Co. Inc., Ch. 14 (1976).
26. H. Kavas, Z. Durmus, M. Senel, S. Kazan, A. Baykal and M.S. Toprak, *Polyhedron*, **29**, 1375 (2010).
27. W.Z. Wang, C.K. Xu, G.H. Wang, Y.K. Liu and C.L. Zheng, *Adv. Mater.*, **14**, 837 (2002).
28. N. Gupta, A. Verma, S.C. Kashyap and D.C. Dube, *J. Magn. Magn. Mater.*, **308**, 137 (2007).
29. G.J. Hutchings, A.A. Mirzaei, R.W. Joyner, M.R.H. Siddiqui and S.H. Taylor, *Catal. Lett.*, **42**, 21 (1996).
30. N.M. Deraz and A. Alarifi, *J. Anal. Appl. Pyrolysis*, **97**, 55 (2012).
31. N.M. Deraz and M.G. Moustafa Fouda, *Int. J. Electrochem. Soc.*, **8**, 2682 (2013).
32. N.M. Deraz and M.G. Moustafa Fouda, *Int. J. Electrochem. Soc.*, **8**, 2756 (2013).
33. G. Blasse, *J. Phys. Chem. Solids*, **27**, 383 (1966).
34. R. Buhl, *J. Phys. Chem. Solids*, **30**, 805 (1969).
35. G.G. Robbrecht and C.M. Henriët-Iserentant, *Phys. Status Solidi*, **41**, K43 (1970).
36. A. Bielanski, K. Dyrek, Z. Kluz, J. Slozynski and T. Tombiasz, *Bull. Acad. Pol. Sci.*, **9**, 657 (1964).
37. R.E. Vandenberghe, G.G. Robbrecht and V.A.M. Brabers, *Mater. Res. Bull.*, **8**, 571 (1973).
38. F. Li, L. Zhang, D.G. Evans and X. Duan, *Colloids Surf. A*, **244**, 169 (2004).
39. E. Elbadraoui, J.L. Baudour, F. Bouree, B. Gillot, S. Fritsch and A. Rousset, *Solid State Ionics*, **93**, 219 (1997).
40. T. Battault, R. Legros and A. Rousset, *J. Eur. Ceram. Soc.*, **15**, 1141 (1995).
41. A. Rousset, *Solid State Ionics*, **84**, 293 (1996).
42. C. Drouet, C. Laberty, J.L.G. Fierro, P. Alphonse and A. Rousset, *Int. J. Inorg. Mater.*, **2**, 419 (2000).
43. A. Navrotsky and O.J. Kleppa, *J. Inorg. Nucl. Chem.*, **29**, 2701 (1967).